JOURNAL OF AGRICULTURAL AND FOOD CHEMISTRY
ARTICLE

J. Agric. Food Chem. 2010, 58, 6119–6125 6119
DOI:10.1021/jf1008617

Stereoselective Conjugation, Transport and Bioactivity of *S*- and *R*-Hesperetin Enantiomers in Vitro

Walter Brand,*[,†,‡] Jia Shao,[†] Elisabeth F. Hoek-van den Hil,[†] Kathelijn N. van Elk,[†] Bert Spenkelink,[†] Laura H. J. de Haan,[†] Maarit J. Rein,[‡] Fabiola Dionisi,[‡] Gary Williamson,[‡,§] Peter J. van Bladeren,[†,‡] and Ivonne M. C. M. Rietjens[†]

[†]Division of Toxicology, Wageningen University, Tuinlaan 5, PO Box 8000, 6703 HE Wageningen, The Netherlands, [‡]Nestlé Research Center, Nestec Ltd., Vers-chez-les-Blanc, PO Box 44, 1000 Lausanne 26, Switzerland, and [§]School of Food Science and Nutrition, University of Leeds, Leeds LS2 9JT, U.K.

The flavanone hesperetin ((±)-4′-methoxy-3′,5,7-trihydroxyflavanone) is the aglycone of hesperidin, which is the major flavonoid present in sweet oranges. Hesperetin contains a chiral C-atom and so can exist as an *S*- and *R*-enantiomer, however, in nature 2*S*-hesperidin and its *S*-hesperetin aglycone are predominant. The present study reports a chiral HPLC method to separate *S*- and *R*-hesperetin on an analytical and semipreparative scale. This allowed characterization of the stereoselective differences in metabolism and transport in the intestine and activity in a selected bioassay of the separated hesperetin enantiomers in in vitro model systems: (1) with human small intestinal fractions containing UDP-glucuronosyl transferases (UGTs) or sulfotransferases (SULTs); (2) with Caco-2 cell monolayers as a model for the intestinal transport barrier; (3) with mouse Hepa-1c1c7 cells transfected with human EpRE-controlled luciferase to test induction of EpRE-mediated gene expression. The results obtained indicate some significant differences in the metabolism and transport characteristics and bioactivity between *S*- and *R*-hesperetin, however, these differences are relatively small. This indicates that for these end points, including intestinal metabolism and transport and EpRE-mediated gene induction, experiments performed with racemic hesperetin may adequately reflect what can be expected for the naturally occurring *S*-enantiomer. This is an important finding since at present hesperetin is only commercially available as a racemic mixture, while it exists in nature mainly as an *S*-enantiomer.

KEYWORDS: Flavonoid; chirality; HPLC; stereoselectivity; conjugation

INTRODUCTION

The flavanone hesperetin ((±)-4′-methoxy-3′,5,7-trihydroxyflavanone) (**Figure 1**) is the aglycone of hesperidin (hesperetin 7-*O*-rutinoside), which is the major flavonoid present in sweet oranges (*Citrus sinensis*) and orange juice but which can also be found in other citrus fruits including lemon, lime, and mandarin and some herbs (*1*). Hesperetin and hesperidin have been reported to provide health beneficial effects, including anticarcinogenic properties and a reduced risk of osteoporosis (*2*−*4*).

Upon ingestion, hesperidin has to be hydrolyzed into hesperetin aglycone by colonic microbiota prior to its absorption. Conversion of the disaccharide hesperidin into the monosaccharide hesperetin 7-*O*-glucoside prior to consumption has been demonstrated to lead to absorption already in the small intestine after deglucosylation by phloridzin hydrolase and/or by facilitated transport into the intestinal cells by a sodium dependent glucose transporter (e.g., SGLT1) followed by intracellular deglucosylation (*5*). In the intestinal cells, hesperetin aglycone can be conjugated by UDP-glucuronosyltransferases (UGTs) and sulfotransferases (SULTs) into glucuronidated and sulfonated metabolites, respectively, which have been found in vivo in both rat and human plasma (*6*, *7*). The intestinal barrier is believed to play a dominant role in the conjugation of hesperetin (*8*) and in its limited bioavailability because of efflux of the metabolites back to the intestinal lumen by ABC transport proteins (*9*, *10*).

Unlike many other classes of flavonoids, flavanones as well as flavanols share a chiral carbon atom in position 2 and therefore exist in an *S*- and *R*-configuration (**Figure 1**). 2*S*-Hesperidin is naturally predominant in citrus fruits (*11*−*13*), and hesperidin is present in fresh, sweet orange juice in an *S*:*R* ratio of at least 92:8 in favor of the 2*S*-epimer (*14*−*16*). Although in nature the 2*S*-epimer of hesperidin, and subsequently the *S*-hesperetin enantiomer, is dominant, hesperetin and hesperidin are currently only commercially available as a mixture of both stereoisomers. As a result, studies on hesperetin and hesperidin generally do not take the chirality into account whereas in theory the two enantiomers may display distinct kinetic and dynamic properties (*17*).

*To whom correspondence should be addressed. Phone: +31-317-482294. Fax: +31-317-484931. E-mail: Walter.Brand@WUR.nl.

Published on Web 05/04/2010

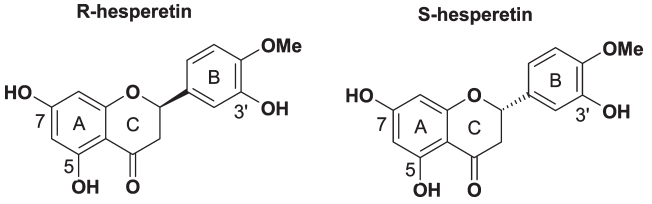

Figure 1. Chemical structure of (−)-*S*- and (+)-*R*-hesperetin (4′-methoxy-3′,5,7-trihydroxyflavanone).

For flavonoids, stereochemical properties have been reported to influence, for example, the bioavailability of the flavanol catechin (*18*), the estrogenic activity of the isoflavone metabolite equol (*19*, *20*), and the plasma and urinary kinetics of hesperetin (*16*, *21*) and may thus very well affect both the intestinal metabolism and transport of hesperetin as well as its biological effects.

Although several studies reported analytical methods to analyze *S*- and *R*-enantiomers of hesperetin, as reviewed by Yáñez et al. (*11*), the kinetic differences of *S*- and *R*-hesperetin were only studied indirectly. After intravenous administration of racemic hesperetin to rats, *R*-hesperetin had a significant 3.3-fold higher area under the serum concentration−time curve (AUC) and a 1.9-fold longer half-life, compared to *S*-hesperetin (after enzymatic hydrolysis of the metabolites in plasma samples) (*16*).

The aim of the present study was to develop a method for separation of *S*- and *R*-hesperetin on an analytical and semipreparative scale using chiral HPLC with α1-acid glycoprotein (AGP) as chiral selector and to characterize differences in the intestinal conjugation and transport, and the activity in a selected bioassay, of the two hesperetin enantiomers in in vitro models. To that end, we performed incubations with microsomal and cytosolic fractions of human small intestine with the separated enantiomers in order to determine the apparent kinetics for glucuronidation and sulfonation of *S*- and *R*-hesperetin. Furthermore, the stereoselective differences in intestinal metabolism and transport were assessed using Caco-2 cell monolayers in a two-compartment transwell system as a model for the intestinal barrier. To test differences in a selected bioassay, *S*- and *R*-hesperetin were tested in a reporter gene based bioassay quantifying EpRE-(electrophile responsive element) mediated activation of gene expression. EpRE-mediated activation of gene expression is considered to contribute to the cancer preventive action of chemoprotective dietary compounds including flavonoids (*22*,*23*).

MATERIALS AND METHODS

Materials. Alamethicin (from *Trichoderma viride*), crude preparation of β-glucuronidase (from *Helix pomatia*) type HP-2, hesperetin (purity ≥95%, batch 015K1099), L-ascorbic acid, and uridine 5′-diphosphoglucuronic acid (UDPGA) were obtained from Sigma (St. Louis, MO), 3′-phosphoadenosine 5′-phosphosulfate (PAPS) from Fluka (Buchs, Switzerland), dimethyl sulfoxide (DMSO), dipotassium hydrogen phosphate trihydrate, EDTA disodium salt dehydrate, glacial acetic acid, hydrochloric acid, potassium dihydrogen phosphate, and sodium acetate trihydrate from Merck (Darmstadt, Germany), acetonitrile, isopropyl alcohol, and methanol from Sigma-Aldrich (Steinheim, Germany), Tris from Invitrogen (Carlsbad, CA), and ammonium acetate and trifluoroacteic acid from J. T. Baker (Philipsburg, NJ). Authentic standards of hesperetin 7-*O*-glucuronide (purity >90%), hesperetin 3′-*O*-glucuronide (purity >90%), and hesperetin 7-*O*-sulfate (purity <50%) were provided by Nestlé Research Center (Lausanne, Switzerland). An orange (*Citrus sinensis*) from South Africa was bought at a local store. All cell culture reagents were purchased from Invitrogen (Paisley, UK). Pooled human small intestinal microsomes (batch MIC318012) and pooled human small intestinal cytosol (batch CYT318004) were purchased from Biopredic (Rennes, France).

Cell Lines. Caco-2 human colon carcinoma cells were obtained from the American Type Culture Collection (Manassas, VA) and were cultured as described earlier (*9*). Passage numbers 39 to 47 were used for the experiments.

Hepa-1c1c7 mouse hepatoma cells stably transfected with the reporter vector pTI(hNQO1-EpRE)Luc+ from Promega (Leiden, The Netherlands) carrying the EpRE from the human NQO1 gene regulatory region between −470 and −448 (5′-AGT CAC AGT GAC TCA GCA GAA TC-3′), coupled to a luciferase reporter gene, were obtained as described previously (*24*). These transfected Hepa-1c1c7 cells will further be referred to as EpRE-LUX cells.

Identification of *S*-Hesperetin. Hesperidin naturally occurs predominantly as the 2*S*-epimer (*14*−*16*). To acquire *S*-hesperetin, 2*S*-hesperidin from an orange (*Citrus sinensis*) was deglycosylated. To this end, freshly prepared orange juice (0.5 mL) was added to 1 mL of nanopure water, 110 μL of 0.78 M sodium acetate (pH 4.8), 100 μL of 0.1 M ascorbic acid, and 200 μL of crude preparation of β-glucuronidase from *Helix pomatia* type HP-2, which also deglycosylates flavanone rutinosides (*16*, *25*), and incubated overnight at 37 °C (*16*, *25*). Then, 1 mL of acetonitrile was added to precipitate the proteins, and the mixture was vortexed for 1 min and centrifuged at 16000*g* for 5 min. The supernatant was collected, the solvent was evaporated under nitrogen gas, and the residue was dissolved in the mobile phase for chiral HPLC analysis.

Chiral HPLC-DAD Analysis. Chiral analyses of hesperetin were performed on an HPLC system consisting of a Waters (Milford, MA) Alliance 2695 separation module connected to a Waters 2996 photodiode array detector (DAD) equipped with a ChromTech (Cheshire, UK) analytical 150 mm × 4 mm Chiral-AGP column connected to a 10 mm × 4 mm guard column. Samples were centrifuged at 16000*g* for 4 min, and 20 μL was injected and isocratically eluted at a flow rate of 0.9 mL/min in 10 mM ammonium acetate (pH 5.0) containing 2% (v/v) isopropyl alcohol, filtered through a membrane filter with a pore size of 0.45 μm from Schleicher and Schuell (Dassel, Germany). The column was equilibrated for 10 min before injection and washed with 15% (v/v) isopropyl alcohol in nanopure water. DAD-UV spectra were detected between 200 and 420 nm, and HPLC chromatograms acquired at 280 nm were used for quantification and presentation.

Semipreparative Separation of *S*- and *R*-Hesperetin. Semipreparative HPLC separation of the *S*- and *R*-enantiomers of hesperetin was performed on an HPLC system consisting of an Uniflows Degasys DG-2410 degasser (Tokyo, Japan), a Waters 600 fluid unit, and a controller connected to a Waters 996 DAD (Milford, MA), equipped with a ChromTech semipreparative 100 mm × 10.0 mm Chiral-AGP column (Cheshire, UK). An injection volume of 100 μL of 500 μM of racemic hesperetin in 25% (v/v) isopropyl alcohol in nanopure water was injected and eluted at a flow rate of 5.6 mL/min in 10 mM ammonium acetate (pH 5.0) containing 2% (v/v) isopropyl alcohol and filtered through a membrane filter with a pore size of 0.45 μm from Schleicher and Schuell (Dassel, Germany). Elution of both hesperetin enantiomers was followed at 280 nm. Fractions containing the separate enantiomers were collected and divided into Eppendorf tubes and freeze-dried. The resulting products were dissolved in a small amount of methanol, pooled, and dried under a flow of nitrogen and redissolved in a small amount of DMSO. To check the enantiomeric purity (>95%), a sample of each preparation, 100-fold diluted with 25% (v/v) isopropyl alcohol in nanopure water, was analyzed by chiral HPLC-DAD. To precisely determine the hesperetin concentration, a 100- or 1000-fold diluted sample of each preparation in 20% acetonitrile (v/v) in 0.1% trifluoroacetic acid in nanopure water was analyzed by a-Chiral HPLC-DAD based on detection at 280 nm using a 10-point linear (R^2 > 0.99) calibration line of relevant concentrations of racemic hesperetin. On the basis of the outcome of this quantification, the separated *S*- and *R*-hesperetin solutions in DMSO were further diluted with DMSO to create 10 mM stock solutions. A sample dissolved in cell culture medium did not demonstrate racemization after incubation at 37 °C for 2 h (data not shown). No other peaks were detected in the chromatograms of the a-Chiral analysis of *S*- or *R*-hesperetin, when chromatograms were analyzed at different wavelengths (data not shown).

Microsomal and Cytosolic Incubations. To study intestinal glucuronidation of *S*- and *R*-hesperetin, incubations with human intestinal microsomes were performed as described before for racemic hesperetin (*26*). The incubation mixtures (total volume 200 μL) contained 10 mM $MgCl_2$,

25 μg/mL alamethicin added from a 200 times concentrated stock solution in methanol (final concentration 0.5% methanol), 0.1 mg/mL microsomal protein, and 1 mM uridine 5′-diphosphoglucuronic acid (UDPGA) in 50 mM Tris-HCl (pH 7.5). The reaction was started by addition of *S*- or *R*-hesperetin from a 200 times concentrated stock solution in DMSO (final concentration 0.5% DMSO) and incubated for 5 min at 37 °C. The reaction was terminated by addition of 50 μL of acetonitrile. Under these conditions, formation of hesperetin glucuronides was linear in time and with the amount of protein (data not shown).

To study intestinal sulfonation of *S*- and *R*-hesperetin, incubations with human intestinal cytosol were performed as described before for racemic hesperetin (*26*). The incubation mixtures (total volume 100 μL) contained 5 mM $MgCl_2$, 0.5 mg/mL cytosolic protein, and 100 μM 3′-phosphoadenosine 5′-phosphosulfate (PAPS) in 50 mM potassium phosphate (pH 7.4). The reaction was started by addition of *S*- or *R*-hesperetin from a 100 times concentrated stock solution in DMSO (final concentration 1% DMSO) and incubated for 5 min at 37 °C. The reaction was terminated by addition of 25 μL of acetonitrile. Under these conditions, formation of hesperetin sulfates was linear in time and with the amount of protein (data not shown).

Metabolism and Transport by Caco-2 Cell Monolayers. Caco-2 cells were cultured in a humidified atmosphere of 5% CO_2 and 95% air at 37 °C and seeded at a density of 1×10^5 cells/cm^2 in Costar 12-well transwell plate inserts from Corning (Corning, NY) with an insert membrane pore size of 0.4 μm and growth area of 1.12 cm^2. The culture medium consisted of Dulbecco's modified Eagle's medium (DMEM) containing 25 mM HEPES buffer (pH 7.4), 4500 mg/mL glucose, L-glutamine, and phenol red, supplemented with 10% (v/v) heat inactivated (30 min at 56 °C) fetal bovine serum, 1% (v/v) minimal essential medium nonessential amino acids (NEAA), and 0.1 mg/mL gentamicin. The medium was changed three times a week. The transport experiment was performed 18−19 days postseeding, for which the monolayers were washed and further incubated with DMEM without phenol red. The integrity of the monolayers was checked by measuring the trans-epithelial electrical resistance (TEER) values with a Millicell ERS volt/ohmmeter from Millipore (Bedford, MA). Only monolayers that demonstrated a TEER value between 500 and 1000 Ω/cm^2 were used. For the experiment, exposure medium was prepared consisting of DMEM (without phenol red) supplemented with 1% (v/v) NEAA and 1 mM L-ascorbic acid, which was filtered through a sterile 0.2 μm filter unit from VWR (West Chester, PA). The monolayers were exposed at the apical side to exposure medium containing 10 μM *S*-hesperetin or *R*-hesperetin (final concentration 0.5% DMSO). Samples of 150 μL were taken from the apical and basolateral side 120 min upon addition, whereafter integrity of the monolayer was reconfirmed. All samples were stored at −80 °C until further HPLC-DAD analysis carried out as described earlier (*9*).

a-Chiral HPLC Analysis. a-Chiral gradient HPLC on a C18 column was used to detect and quantify the amounts of hesperetin, hesperetin 7-*O*-glucuronide, hesperetin 3′-*O*-glucuronide, hesperetin 7-*O*-sulfate, and hesperetin 3′-*O*-sulfate using methods previously described (*9*, *26*).

Enzyme Kinetics. To determine the kinetics for glucuronidation and sulfonation, microsomal and cytosolic incubations were performed as described above by varying the concentration of *S*- or *R*-hesperetin from 1 to 50 μM. Under the applied conditions, the formation of hesperetin 7-*O*-glucuronide, hesperetin 3′-*O*-glucuronide, hesperetin 7-*O*-sulfate, and hesperetin 3′-*O*-sulfate conjugates was linear in time and with the amount of microsomal protein added (data not shown). The apparent maximum velocity ($V_{max(app)}$) and apparent Michaelis−Menten constant ($K_{m(app)}$) for the formation of the different phase II metabolites of *S*- and *R*-hesperetin were determined by fitting the data to the Michaelis−Menten steady-state model $v = V_{max}/(1 + (K_m/[S]))$, with [S] being the hesperetin concentration, using the LSW data analysis toolbox (version 1.1.1) from MDL Information Systems (San Ramon, CA).

EpRE-Lux Assay. EpRE-mediated induction of gene expression by *S*- and *R*-hesperetin was tested using the EpRE-LUX luciferase reporter gene assay as described earlier (*24*, *27*). The EpRE-LUX cells were cultured in alpha modified Eagle's medium supplemented with 10% fetal bovine serum, 50 μg/mL gentamicin, and 0.5 mg/mL G418 from Duchefa (Haarlem, The Netherlands), in a humidified atmosphere of 5% CO_2 and 95% air at 37 °C. Cell suspension (100 μL) with a density of 3×10^5 cells/ml was seeded per well in a 96 well view-plate (Corning, NY) and incubated for 24 h, whereafter the cells had attached to the bottom and formed a confluent monolayer. The plates were exposed to different concentrations of *S*- or *R*-hesperetin. To this end, the culture medium was removed and replaced by 100 μL of medium containing hesperetin at the required concentration (0.5% DMSO). The plates were incubated for another 24 h, whereafter the cells were washed with 0.5 × PBS and lysed by addition of low salt buffer (10 mM Tris, 2 mM DTT, and 2 mM *trans*-1,2-diaminocyclohexane-*N*,*N*,*N*′,*N*′-tetra-acetic acid monohydrate, pH 7.8). After lysis, luciferase reagent (20 mM tricine, 1.07 mM $(MgCO_3)_4$-$Mg(OH)_2$, 2.67 mM $MgSO_4$, 0.1 mM EDTA, 2 mM DTT, 0.47 mM D-luciferin, 5 mM ATP; pH 7.8) was added and the luciferase activity was measured using a Luminoskan Ascent luminometer from Thermo Electron Corporation (Helsinki, Finland).

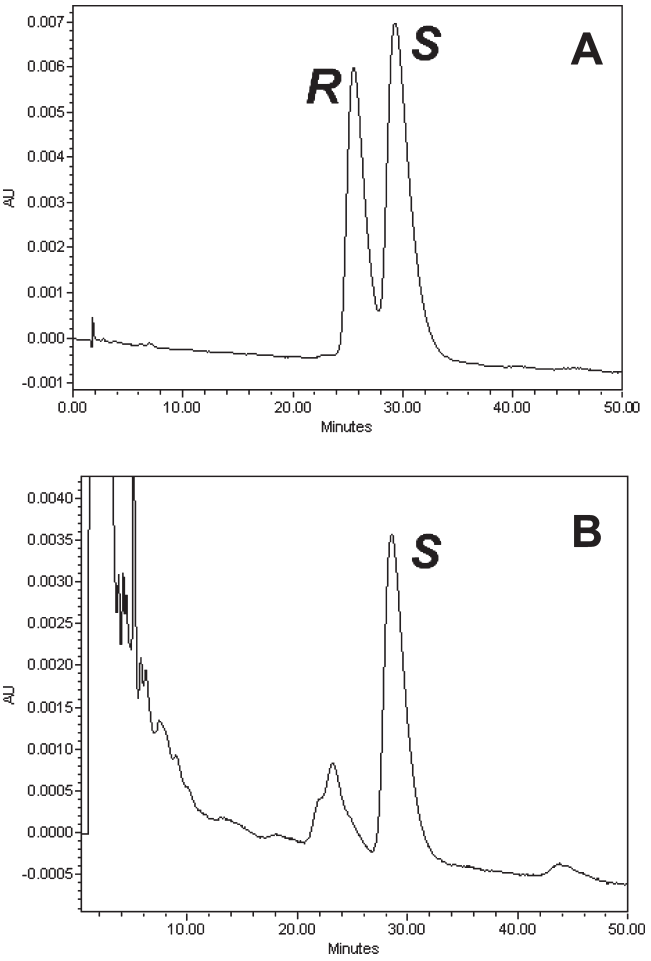

Figure 2. Chiral HPLC chromatograms of (**A**) racemic hesperetin, (**B**) hesperetin resulting from deglycosylation of the 2*S*-hesperidin epimer from citrus.

RESULTS

Analytical and Semipreparative Chiral HPLC-DAD Analyses. **Figure 2A** depicts a chromatogram of the analytical chiral HPLC analysis of racemic hesperetin, demonstrating the two enantiomers at retention times (t_R) 25.5 and 29.0 min in a 41:59 ratio. Both peaks demonstrated equivalent UV spectra, with a UV_{max} at 285.9 nm. The limit of detection, defined as the lowest concentration which can be detected (signal-to-noise ratio 3) of this method was 0.6 μM, the limit of quantification, defined as the lowest concentration which can be quantitatively determined (signal-to-noise ratio 10) was 2 μM. To identify the *S*- and *R*-hesperetin enantiomers, hesperidin from fresh orange juice, mainly present as 2*S*-epimer, was deglycosylated to yield predominantly *S*-hesperetin and analyzed (**Figure 2B**). The peak at t_R 29.0 min

(UV_{max} = 285.9 nm), was dominant in the hydrolyzed citrus sample identifying the corresponding metabolite as *S*-hesperetin. *S*- and *R*-hesperetin were successfully separated on a semipreparative scale and concentrated, yielding sufficient amounts to perform small scale in vitro experiments. The racemic purity after vacuum concentration and pooling of the collected samples was >95% for both *S*- and *R*-hesperetin.

Microsomal Glucuronidation. Hesperetin is glucuronidated by small intestinal microsomes into hesperetin 7-*O*-glucuronide and 3′-*O*-glucuronide metabolites (*26*). The apparent V_{max} and K_m values derived from the concentration dependent formation of *S*-hesperetin 7-*O*-glucuronide and *S*-hesperetin 3-*O*-glucuronide (**Figure 3A**), and *R*-hesperetin 7-*O*-glucuronide and *R*-hesperetin 3′-*O*-glucuronide (**Figure 3B**) by human small intestinal microsomes, are presented in **Table 1**, as well as the apparent catalytic efficiencies (V_{max}/K_m). For comparison, **Table 1** also presents the kinetic data obtained previously for racemic hesperetin (*26*). For the glucuronidation of both hesperetin enantiomers, the relative contribution of the conjugation at position 7 and 3′ is comparable. However, the affinity was higher (K_m lower) for the glucuronidation of *S*-hesperetin as compared to the glucuronidation of *R*-hesperetin. Together with a slightly higher capacity (V_{max}), this results in a 5.2-fold higher catalytic efficiency for the glucuronidation of *S*-hesperetin compared to *R*-hesperetin (**Table 1**). The catalytic efficiencies obtained for 7-*O*-glucuronide formation from *S*- and *R*-hesperetin were respectively 2.7-fold higher and 2.5-fold lower than the catalytic efficiencies observed with the racemic mixture, and the catalytic efficiencies obtained for 3′-*O*-glucuronide formation from *S*- and *R*-hesperetin were respectively 2.5-fold higher and 1.6-fold lower compared to the catalytic efficiencies observed with the racemic mixture.

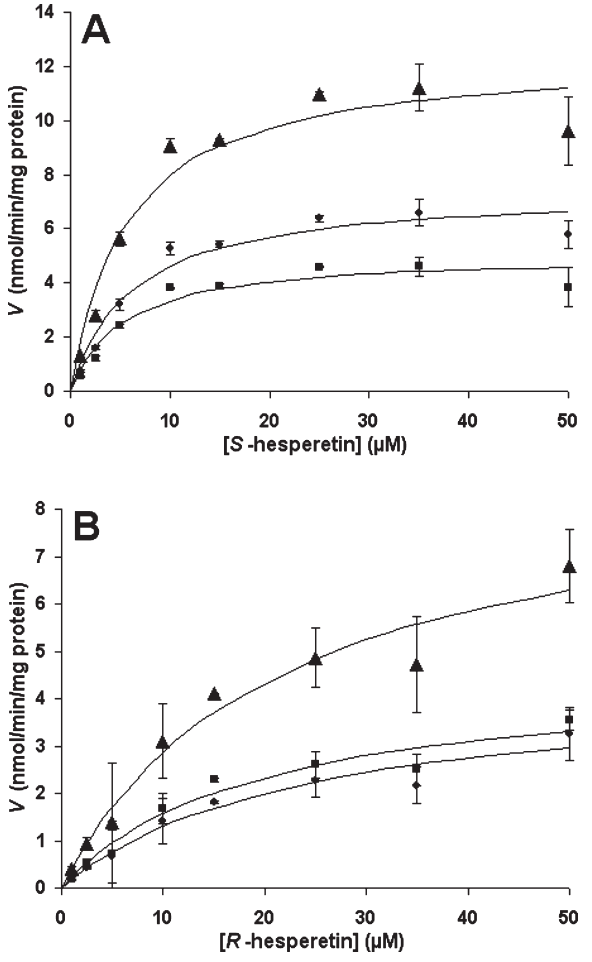

Figure 3. Concentration dependent formation of hesperetin 7-*O*-glucuronide (●), hesperetin 3′-*O*-glucuronide (■), and total hesperetin glucuronides (▲) from *S*-hesperetin (**A**) and *R*-hesperetin (**B**) enantiomers by human small intestinal microsomes. Data points represent average activities of two measurements ± SD.

Cytsosolic Sulfonation. Hesperetin is sulfonated by human small intestinal cytosol into hesperetin 3′-*O*-sulfate and 7-*O*-sulfate metabolites (*26*). The apparent V_{max} and K_m values derived from the concentration dependent formation of *S*-hesperetin 3′-*O*-sulfate and *S*-hesperetin 7-*O*-sulfate (**Figure 4A**), and *R*-hesperetin 3′-*O*-sulfate and *R*-hesperetin 7-*O*-sulfate (**Figure 4B**) by human small intestinal microsomes are shown in **Table 2**, as well as the apparent catalytic efficiencies (V_{max}/K_m). For comparison, **Table 2** also presents the kinetic data obtained previously for racemic hesperetin (*26*). Both hesperetin enantiomers are predominantly sulfonated at position 3′, although the capacity and the relative contribution of the formation of 7-*O*-sulfonation to the total sulfonation of *R*-hesperetin is higher as compared with the sulfonation of *S*-hesperetin (**Table 2**). The catalytic efficiency obtained for 3′-*O*-sulfate formation from *S*- and *R*-hesperetin were respectively 1.2-fold lower and 1.5-fold higher than the catalytic efficiencies observed with the racemic mixture, and the catalytic efficiency obtained for 7′-*O*-sulfate formation from *S*- and *R*-hesperetin were respectively equal and 2.8-fold higher compared to the catalytic efficiencies observed with the racemic mixture (*26*).

Metabolism and Transport by Caco-2 Cell Monolayers. Caco-2 cell monolayers apically exposed to hesperetin metabolize it into hesperetin 7-*O*-glucuronide and hesperetin 7-*O*-sulfate, which are predominantly transported to the apical side of the monolayer (*9*). **Figure 5** shows the percentages of the applied amount of *S*-hesperetin or *R*-hesperetin that is metabolized into 7-*O*-glucuronide or 7-*O*-sulfate metabolites as well as the percentage which remained unmetabolized and the disposition of the metabolites to the apical or basolateral side of the Caco-2 cell monolayer. Exposure to *R*-hesperetin resulted in a significantly ($p < 0.001$) higher amount of hesperetin 7-*O*-sulfate formed, amounting to

Table 1. Apparent V_{max} (±SEM), K_m (±SEM), and Catalytic Efficiency for the Glucuronidation of *S*- and *R*-Hesperetin by Human Small Intestinal Microsomes ($n = 2$)[a]

	S-hesperetin			*R*-hesperetin			racemic hesperetin[b]		
conjugation reaction	K_m(app) (μM)	V_{max}(app) (nmol min^{-1} mg protein^{-1})	catalytic efficiency (μL min^{-1} mg protein^{-1})	K_m(app) (μM)	V_{max}(app) (nmol min^{-1} mg protein^{-1})	catalytic efficiency (μL min^{-1} mg protein^{-1})	K_m(app) (μM)	V_{max}(app) (nmol min^{-1} mg protein^{-1})	catalytic efficiency (μL min^{-1} mg protein^{-1})
glucuronidation (total)	5.7 ± 1.7	12.5 ± 0.99	2189	21.3 ± 6.5	8.95 ± 1.24	420	7.3 ± 1.4	6.26 ± 1.67	858
7-*O*-glucuronidation	6.1 ± 1.6	7.43 ± 0.56	1224	24.0 ± 8.0	4.40 ± 0.69	183	8.3 ± 1.9	3.80 ± 0.50	458
3′-*O*-glucuronidation	5.2 ± 1.7	5.08 ± 0.43	971	18.9 ± 6.1	4.55 ± 0.63	240	6.4 ± 1.2	2.49 ± 0.49	391

[a] Catalytic efficiency was calculated as $V_{max(app)}/K_{m(app)}$. [b] The kinetic data for racemic hesperetin are taken from our previous work (*26*).

129% (at the apical plus basolateral side) of the amount of hesperetin 7-*O*-sulfate formed upon exposure to *S*-hesperetin (**Figure 5**). The total amount of *R*-hesperetin 7-*O*-glucuronide formed was 8% lower compared to the amount of S-hesperetin 7-*O*-glucuronide formed, and this difference was not significant (**Figure 5**). The total amount of hesperetin metabolites and/or aglycone transported over the Caco-2 monolayer did not differ significantly for *S*- and *R*-hesperetin.

Activation of EpRE-Controlled Gene Expression by Hesperetin. **Figure 6** shows the concentration dependent induction of EpRE-mediated luciferase expression by *S*-hesperetin and *R*-hesperetin. Exposure to both hesperetin enantiomers resulted in a dose dependent induction of EpRE mediated gene expression: exposure to *S*-hesperetin led to an 8.2-fold (±0.6) induction at 50 μM, and exposure to *R*-hesperetin to a maximum induction of 6.0-fold (±0.2) at 25 μM and higher (**Figure 6**). Although at some of the concentrations significant differences are found between the induction factors by *S*- and *R*-hesperetin, the overall induction however, especially at lower, and thus physiologically relevant, concentrations does not demonstrate notable differences in activation of EpRE mediated gene expression between both hesperetin enantiomers.

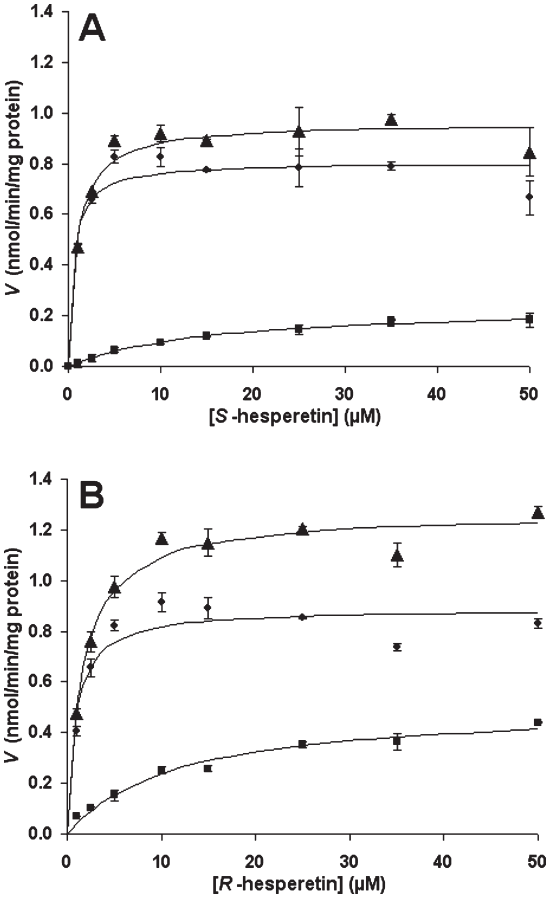

Figure 4. Concentration dependent formation of hesperetin 7-*O*-sulfate (■), hesperetin 3′-*O*-sulfate (●), and total hesperetin sulfates (▲) from *S*-hesperetin (**A**) and *R*-hesperetin (**B**) enantiomers by human small intestinal cytosol. Data points represent average activities of two measurements ± SD.

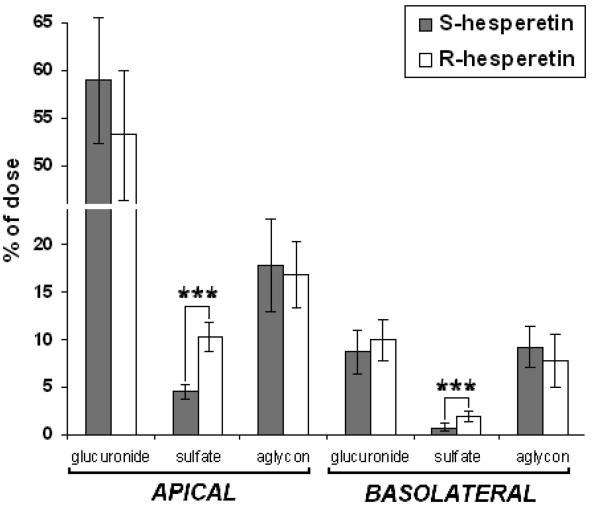

Figure 5. Amount of hesperetin 7-*O*-glucuronide (glucuronide), hesperetin 7-*O*-sulfate (sulfate), and hesperetin aglycone detected at the apical and basolateral side of Caco-2 cell monolayers incubated for 120 min with 10 μM *S*-hesperetin or *R*-hesperetin added to the apical side. Mean ± SD values shown (n = 8). ***, $p < 0.001$ significantly different.

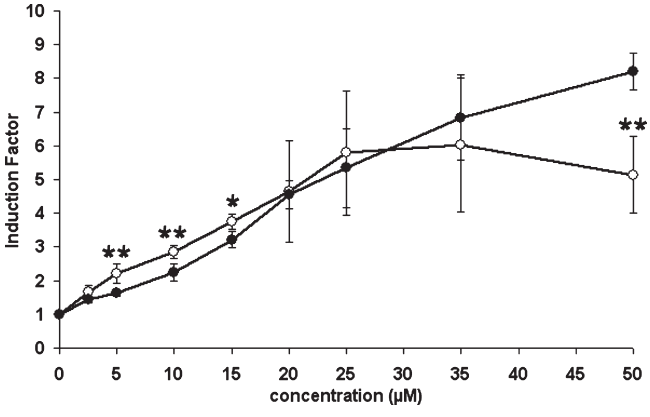

Figure 6. Induction of EpRE-mediated gene transcription by *R*-hesperetin (○) and *S*-hesperetin (●). Data are presented as mean (±SD) (n = 4). *, $p < 0.05$; **, $p < 0.01$ significantly different compared with the induction by corresponding the corresponding concentration of the other hesperetin enantiomer.

Table 2. Apparent V_{max} (±SEM), K_m (±SEM), and Catalytic Efficiency for the Sulfonation of *S*- and *R*-Hesperetin by Human Small Intestinal Cytosol (n = 2)[a]

	S-hesperetin			*R*-hesperetin			racemic hesperetin[b]		
conjugation reaction	K_m(app) (μM)	V_{max}(app) (nmol min^{-1} mg protein^{-1})	catalytic efficiency (μL min^{-1} mg protein^{-1})	K_m(app) (μM)	V_{max}(app) (nmol min^{-1} mg protein^{-1})	catalytic efficiency (μL min^{-1} mg protein^{-1})	K_m(app) (μM)	V_{max}(app) (nmol min^{-1} mg protein^{-1})	catalytic efficiency (μL min^{-1} mg protein^{-1})
sulfonation (total)	0.9 ± 0.2	0.96 ± 0.03	1067	1.6 ± 0.2	1.27 ± 0.04	803	0.8 ± 0.1	0.90 ± 0.29	1082
7-*O*-sulfonation	15.6 ± 2.5	0.25 ± 0.03	16	11.5 ± 2.1	0.51 ± 0.04	44	9.1 ± 1.5	0.14 ± 0.04	16
3′-*O*-sulfonation	0.6 ± 0.2	0.80 ± 0.03	1455	0.9 ± 0.3	0.89 ± 0.04	1000	0.6 ± 0.2	0.79 ± 0.14	1240

[a] Catalytic efficiency was calculated as $V_{max(app)}/K_{m(app)}$. [b] The kinetic data for racemic hesperetin are taken from our previous work (*26*).

DISCUSSION

Although hesperidin naturally exists mainly as the 2*S*-epimer, which upon intake is subsequently transformed into *S*-hesperetin, practically all research on hesperidin and hesperetin using "pure" compounds is actually on racemic mixtures, which are currently the only forms of hesperidin and hesperetin commercially available. Stereochemical differences have been proven to affect the bioavailability of flavonoids, as was shown for example for catechin. (+)-Catechin (2*R*,3*S*-catechin) has been demonstrated to be up to 2.1-fold more bioavailable compared to (−)-catechin (2*S*,3*R*-catechin), partly due to increased intestinal absorption (*18*).

To study the differences between the "natural" *S*-hesperetin and *R*-hesperetin, the present paper reports a method to separate both enantiomers on an analytical and semipreparative scale, allowing small-scale in vitro experiments with the separated enantiomers. This allowed characterization of possible differences in intestinal metabolism and transport and the activity in a selected bioassay of *S*- and *R*-hesperetin, by incubating *S*- or *R*-hesperetin with human small intestinal microsomes and cytosol and cofactors for phase II conjugation, with Caco-2 cell monolayers in a transwell transport model and with a transfected cell line to test induction of EpRE-mediated gene expression.

Although the results obtained indicate some significant differences in metabolism, the differences in the metabolism and transport of the two hesperetin enantiomers are relatively small. The higher affinity and capacity toward *S*-hesperetin resulted in an overall 5.2-fold higher catalytic efficiency for the formation of *S*-hesperetin glucuronides as compared to *R*-hesperetin glucuronides by human small intestinal microsomes (**Table 1**). The differences between the sulfonation kinetics of *S*-hesperetin and *R*-hesperetin are marginal, although the capacity for the formation of 7-*O*-sulfate from *R*-hesperetin is 2.8-fold higher compared with the formation of 7-*O*-sulfate from *S*-hesperetin (**Table 2**, **Figure 4**). Although relatively small, together these kinetic differences might explain the increased formation of hesperetin 7-*O*-sulfate and reduced formation of hesperetin 7-*O*-glucuronide by Caco-2 cell monolayers exposed to *R*-hesperetin as compared to monolayers exposed to *S*-hesperetin (**Figure 5**).

Differences in the kinetics between *S*-hesperetin and *R*-hesperetin have been observed indirectly in vivo after intravenous administration of racemic hesperetin (20 mg/kg bodyweight (bw)) to male Sprague−Dawley rats, demonstrating a significant ($p < 0.05$) 3.2-fold higher area under the serum concentration−time curve (AUC) and 1.9-fold ($p < 0.05$) longer serum half-life for *R*-hesperetin compared to *S*-hesperetin, which had a 3.3-fold ($p < 0.05$) higher total clearance from serum (*16*). The cumulative urinary excretion of *R*-hesperetin was 2.3-fold ($p < 0.05$) higher compared to *S*-hesperetin (*16*). In an earlier study, however, oral administration of racemic hesperidin (200 mg/kg bw) to a single rat revealed only slightly (∼15%) increased cumulative 24 h urinary excretion of *R*-hesperetin compared to *S*-hesperetin, while the cumulative urinary excretion of *R*-hesperetin compared to *S*-hesperetin was only ∼20% lower following the administration of orange juice (containing 7.3 mg/kg bw hesperidin in an *S*:*R* ratio of 6.8:1) to a healthy volunteer (*21*).

Although several of these effects appeared significant, they were moderate in size, showing, similar to the observations in the present study, differences between the kinetic parameters for the *S*- and *R*-enantiomer of less than 5-fold. In addition, the differences never resulted in the complete absence of a biochemical pathway or kinetic route for one of the hesperetin enantiomers. From this it is concluded that kinetic data obtained with the racemic mixture do give insight into what may happen to the naturally predominant *S*-enantiomer of hesperetin. It is of interest to note that interindividual variation in kinetics may be in the same order of magnitude as or even larger than the differences now observed between *S*- and *R*-hesperetin.

In addition to possible differential kinetics for *S*- and *R*-hesperetin, it is of interest to study whether different hesperetin enantiomers would lead to different biological effects. It has been reported for instance that stereochemical differences greatly affect the estrogenic activity of the isoflavone metabolite equol: *S*(−)-equol demonstrated high affinity for estrogen receptor ERβ (K_i = 0.73 nM), whereas *R*(+)-equol had a K_i of only 15.4 nM (*19*).

It has been reported that flavonols and catechins can activate EpRE mediated gene expression because of their pro-oxidant properties under certain conditions (*27*, *28*) by which these flavonoids could exert their chemopreventive action (*23*, *27*). The present study revealed that, at physiologically relevant concentrations, *S*- and *R*-hesperetin were both able to induce EpRE mediated gene expression to a similar extent (**Figure 6**). However, this assay represents only one of the possible mechanisms by which hesperetin could exert biological effects.

In conclusion, in the case of hesperetin, whenever differences were observed in the kinetics of *S*- and *R*-hesperetin, they turned out to be moderate. The most explicit difference found was the 5.2-fold difference in the catalytic efficiency for the glucuronidation of *S*-hesperetin compared to *R*-hesperetin. However, the differences never resulted in the complete absence of a biochemical pathway or kinetic route for one of the hesperetin enantiomers. Also, in a selected bioassay, the two enantiomers were equally active. Taken together, it is concluded that for the end points tested, including intestinal metabolism and transport and EpRE-mediated gene induction, experiments performed with racemic hesperetin may adequately reflect what can be expected for the naturally occurring *S*-enantiomer. This is an important finding since at present hesperetin is only commercially available as a racemic mixture, while it exists in nature mainly as an *S*-enantiomer.

ABBREVIATIONS USED

ABC, ATP binding cassette; AGP, α_1-acid glycoprotein; bw, body weight; DAD, diode array detector; DMEM, Dulbecco's modified Eagle's medium; DMSO, dimethyl sulfoxide; EpRE, electrophile-responsive element; NEAA, nonessential amino acids; PAPS, 3′-phosphoadenosine 5′-phosphosulfate; SD, standard deviation; SEM, standard error of the mean; SGLT1, sodium-glucose cotransporter 1; SULT, sulfotransferase; TEER, trans-epithelial electrical resistance; t_R, retention time; UDPGA, uridine 5′-diphosphoglucuronic acid; UGT, UDP-glucuronosyltransferase.

LITERATURE CITED

(1) Tomás-Barberán, F. A.; Clifford, M. N. Flavanones, chalcones and dihydrochalcones—nature, occurrence and dietary burden. *J. Sci. Food Agric.* **2000**, *80*, 1073–1080.

(2) Chiba, H.; Uehara, M.; Wu, J.; Wang, X.; Masuyama, R.; Suzuki, K.; Kanazawa, K.; Ishimi, Y. Hesperidin, a citrus flavonoid, inhibits bone loss and decreases serum and hepatic lipids in ovariectomized mice. *J. Nutr.* **2003**, *133*, 1892–1897.

(3) Garg, A.; Garg, S.; Zaneveld, L. J. D.; Singla, A. K. Chemistry and pharmacology of the citrus bioflavonoid hesperidin. *Phytother. Res.* **2001**, *15*, 655–669.

(4) Horcajada, M. N.; Habauzit, V.; Trzeciakiewicz, A.; Morand, C.; Gil-Izquierdo, A.; Mardon, J.; Lebecque, P.; Davicco, M. J.; Chee, W. S. S.; Coxam, V.; Offord, E. Hesperidin inhibits ovariectomized-induced osteopenia and shows differential effects on bone mass and strength in young and adult intact rats. *J. Appl. Physiol.* **2008**, *104*, 648–654.

(5) Nielsen, I. L. F.; Chee, W. S. S.; Poulsen, L.; Offord-Cavin, E.; Rasmussen, S. E.; Frederiksen, H.; Enslen, M.; Barron, D.; Horcajada, M.-N.; Williamson, G. Bioavailability is improved by enzymatic modification of the citrus flavonoid hesperidin in humans: a randomized, double-blind, crossover trial. *J. Nutr.* **2006**, *136*, 404–408.

(6) Matsumoto, H.; Ikoma, Y.; Sugiura, M.; Yano, M.; Hasegawa, Y. Identification and quantification of the conjugated metabolites derived from orally administered hesperidin in rat plasma. *J. Agric. Food Chem.* **2004**, *52*, 6653–6659.

(7) Mullen, W.; Archeveque, M.-A.; Edwards, C. A.; Matsumoto, H.; Crozier, A. Bioavailability and metabolism of orange juice flavanones in humans: impact of a full-fat yogurt. *J. Agric. Food Chem.* **2008**, *56*, 11157–11164.

(8) Silberberg, M.; Morand, C.; Mathevon, T.; Besson, C.; Manach, C.; Scalbert, A.; Remesy, C. The bioavailability of polyphenols is highly governed by the capacity of the intestine and of the liver to secrete conjugated metabolites. *Eur. J. Nutr.* **2006**, *45*, 88–96.

(9) Brand, W.; Van der Wel, P. A. I.; Rein, M. J.; Barron, D.; Williamson, G.; Van Bladeren, P. J.; Rietjens, I. M. C. M. Metabolism and transport of the citrus flavonoid hesperetin in Caco-2 cell monolayers. *Drug Metab. Dispos.* **2008**, *36*, 1794–1802.

(10) Liu, Z.; Hu, M. Natural polyphenol disposition via coupled metabolic pathways. *Expert Opin. Drug Metab. Toxicol.* **2007**, *3*, 389–406.

(11) Yáñez, J. A.; Andrews, P. K.; Davies, N. M. Methods of analysis and separation of chiral flavonoids. *J. Chromatogr. B: Anal. Technol. Biomed. Life Sci.* **2007**, *848*, 159–181.

(12) Arakawa, H.; Nakazaki, M. Absolute configuration of (−)hesperetin and (−)liquiritigenin. *Chem. Ind.* **1960**, 73.

(13) Arakawa, H.; Nakazaki, M. Die absolute Konfigurationen der optisch aktiven Flavanone. *Liebigs Ann. Chem.* **1960**, *636*, 111–117.

(14) Aturki, Z.; Brandi, V.; Sinibaldi, M. Separation of flavanone-7-*O*-glycoside diastereomers and analysis in citrus juices by multidimensional liquid chromatography coupled with mass spectrometry. *J. Agric. Food Chem.* **2004**, *52*, 5303–5308.

(15) Gel-Moreto, N.; Streich, R.; Galensa, R. Chiral separation of diastereomeric flavanone-7-*O*-glycosides in citrus by capillary electrophoresis. *Electrophoresis* **2003**, *24*, 2716–2722.

(16) Yáñez, J. A.; Remsberg, C. M.; Miranda, N. D.; Vega-Villa, K. R.; Andrews, P. K.; Davies, N. M. Pharmacokinetics of selected chiral flavonoids: hesperetin, naringenin and eriodictyol in rats and their content in fruit juices. *Biopharm. Drug Dispos.* **2008**, *29*, 63–82.

(17) Ariëns, E. J. Stereochemistry, a basis for sophisticated nonsense in pharmacokinetics and clinical pharmacology. *Eur. J. Clin. Pharmacol.* **1984**, *26*, 663–668.

(18) Donovan, J. L.; Crespy, V.; Oliveira, M.; Cooper, K. A.; Gibson, B. B.; Williamson, G. (+)-Catechin is more bioavailable than (−)-catechin: relevance to the bioavailability of catechin from cocoa. *Free Radical Res.* **2006**, *40*, 1029–1034.

(19) Setchell, K. D. R.; Clerici, C.; Lephart, E. D.; Cole, S. J.; Heenan, C.; Castellani, D.; Wolfe, B. E.; Nechemias-Zimmer, L.; Brown, N. M.; Lund, T. D.; Handa, R. J.; Heubi, J. E. *S*-Equol, a potent ligand for estrogen receptor beta, is the exclusive enantiomeric form of the soy isoflavone metabolite produced by human intestinal bacterial flora. *Am. J. Clin. Nutr.* **2005**, *81*, 1072–1079.

(20) Setchell, K. D. R.; Zhao, X.; Jha, P.; Heubi, J. E.; Brown, N. M. The pharmacokinetic behavior of the soy isoflavone metabolite *S*-(−)equol and its diastereoisomer *R*-(+)equol in healthy adults determined by using stable-isotope-labeled tracers. *Am. J. Clin. Nutr.* **2009**, *90*, 1029–1037.

(21) Yáñez, J. A.; Teng, X. W.; Roupe, K. A.; Davies, N. M. Stereospecific high-performance liquid chromatographic analysis of hesperetin in biological matrices. *J. Pharm. Biomed. Anal.* **2005**, *37*, 591–595.

(22) Chen, C.; Kong, A. N. Dietary chemopreventive compounds and ARE/EpRE signaling. *Free Radical Biol. Med.* **2004**, *36*, 1505–1516.

(23) Galati, G.; O'Brien, P. J. Potential toxicity of flavonoids and other dietary phenolics: significance for their chemopreventive and anticancer properties. *Free Radical Biol. Med.* **2004**, *37*, 287–303.

(24) Boerboom, A. M. J. F.; Vermeulen, M.; Van der Woude, H.; Bremer, B. I.; Lee-Hilz, Y. Y.; Kampman, E.; Van Bladeren, P. J.; Rietjens, I. M. C. M.; Aarts, J. M. M. J. G. Newly constructed stable reporter cell lines for mechanistic studies on electrophile-responsive element-mediated gene expression reveal a role for flavonoid planarity. *Biochem. Pharmacol.* **2006**, *72*, 217–226.

(25) Erlund, I.; Meririnne, E.; Alfthan, G.; Aro, A. Plasma kinetics and urinary excretion of the flavanones naringenin and hesperetin in humans after ingestion of orange juice and grapefruit juice. *J. Nutr.* **2001**, *131*, 235–241.

(26) Brand, W.; Boersma, M. G.; Bik, H.; Hoek-van den Hil, E. F.; Vervoort, J.; Barron, D.; Meinl, W.; Glatt, H.; Williamson, G.; Van Bladeren, P. J.; Rietjens, I. M. C. M. Phase II metabolism of hesperetin by individual UDP-glucuronosyltransferases and sulfotransferases and rat and human tissue samples. *Drug Metab. Dispos.* **2010**, *38*, 617–625.

(27) Lee-Hilz, Y. Y.; Boerboom, A. M. J. F.; Westphal, A. H.; Berkel, W. J. H.; Aarts, J. M. M. J. G.; Rietjens, I. M. C. M. Pro-oxidant activity of flavonoids induces EpRE-mediated gene expression. *Chem. Res. Toxicol.* **2006**, *19*, 1499–1505.

(28) Muzolf-Panek, M.; Gliszczyńska-Swigło, A.; de Haan, L.; Aarts, J. M. M. J. G.; Szymusiak, H.; Vervoort, J. M.; Tyrakowska, B.; Rietjens, I. M. C. M. Role of catechin quinones in the induction of EpRE-mediated gene expression. *Chem. Res. Toxicol.* **2008**, *21*, 2352–2360.

Received for review March 3, 2010. Revised manuscript received April 14, 2010. Accepted April 26, 2010. This study was supported by a research grant from Nestlé Research Center (Lausanne, Switzerland).